ELSEVIER

Journal of Nuclear Materials 290–293 (2001) 593–597

journal of nuclear materials

www.elsevier.nl/locate/jnucmat

Analysis of SOL behaviour in JET MkIIGB using an advanced onion-skin solver (OSM2)

W. Fundamenski [a,*], S.K. Erents [a], G.F. Matthews [a], A.V. Chankin [a], V. Riccardo [a], P.C. Stangeby [b], J.D. Elder [b]

[a] *EURATOM/UKAEA Fusion Association, Culham Science Centre, Abingdon, Oxon OX14 3DB, UK*
[b] *Institute for Aerospace Studies, University of Toronto, 4925 Dufferin St., Toronto, Ont., Canada M3H 5T6*

Abstract

Interpretative modelling of the JET SOL plasma using the onion-skin method (OSM) has provided valuable insights into relationships between edge plasma parameters and information about the anomalous cross-field energy transport coefficients. The method relies on solving the plasma transport equations along individual flux surfaces, and adjusting the cross-field source terms to best match the Langmuir target probe profiles. In this paper, an improved solver (OSM2) is described and three sets of results are presented: code–code comparison with EDGE2D, code–experiment comparison with reciprocating probe (RCP) data on JET MkIIGB, and detailed simulation of a 12 MW ELMy H-mode on MkIIGB. © 2001 Published by Elsevier Science B.V.

Keywords: 2-D model; Scrape-off layer (SOL); Divertor physics; Divertor modelling

1. Introduction

Edge plasma analysis plays an important role in all tokamak experiments for reasons of power and particle exhaust, impurity generation and transport, and the L–H transition and its effect on confinement (including ITB behaviour). The standard approach of edge plasma analysis involves a solution of transport equations in a 2-D poloidal geometry, with constraints on separatrix power and density as well as specification of radial transport coefficients. This approach suffers from practical disadvantages when applied to interpretation of experiments (related mainly to lengthy parameter searches required to match diagnostic profiles). An alternative approach, termed the onion-skin method (OSM) has in the past shown much promise as an interpretive tool. Below, recent developments in OSM modelling are presented, and the OSM2/NIMBUS code is applied to three case studies: code–code comparison with EDGE2D/NIMBUS, code–experiment comparison with reciprocating probe (RCP) data on JET MkIIGB, and simulation of a 12 MW ELMy H-mode discharge on JET MkIIGB with target power profiles measured using an X-point shift method.

2. Onion-skin method (OSM)

OSM relies on solving the plasma transport equations (in the 21-moment approximation) along individual flux surfaces with the cross-field divergences replaced by simpler source terms and varied to best match selected diagnostic data (in the simplest case, the target Langmuir probe profiles). As an interpretative tool, it has two clear advantages over the standard 2-D approach: (1) speed (by circumventing the need for lengthy parameter searches to match the diagnostic data, convergence times are reduced by two to three orders of magnitude, with the potential for inter-shot analysis), (2) no assumptions about the nature of anomalous transport $(D_\perp, \eta_\perp, \chi_\perp)$. We can represent this schematically as,

* Corresponding author. Tel.: +44-1235 464946.
E-mail address: wfund@jet.uk (W. Fundamenski).

0022-3115/01/$ - see front matter © 2001 Published by Elsevier Science B.V.
PII: S0022-3115(00)00585-7

$$\frac{\partial U}{\partial t}+\nabla_{\parallel}(F_{\parallel}+G_{\parallel})+\nabla_{\wedge}(F_{\wedge}+G_{\wedge})+\nabla_{\perp}(F_{\perp}+G_{\perp})=Q[U]$$
$$\Downarrow$$
$$\frac{\partial U}{\partial t}+\nabla_{\parallel}(F_{\parallel}+G_{\parallel})+\nabla_{\wedge}(F_{\wedge}+G_{\wedge})- \quad Q_{\perp}[U] \quad =Q[U], \tag{1}$$

where U contains the state variables, F the convective fluxes, G the diffusive/viscous/conductive fluxes, and Q the volumetric sources ($\parallel$, $\wedge$ and $\perp$ represent the parallel, diamagnetic and perpendicular directions). In both cases, the parallel physics and target boundary conditions are identical, with only the cross-field terms affected; both methods produce fully 2-D edge plasma profiles. The necessary condition for OSM to work is that the solution be only weakly sensitive to the parallel distribution of the cross-field terms; this may be formulated as a variational principle

$$\left|\frac{Q_{\perp}}{U}\left(\frac{\delta U}{\delta Q_{\perp}}\right)_{\langle Q_{\perp}\rangle}\right|\ll 1, \quad \langle Q_{\perp}\rangle\equiv\frac{1}{L_{\parallel}}\int_0^{L_{\parallel}}Q_{\perp}[U(s_{\parallel})]\,\mathrm{d}s_{\parallel},$$
$$\therefore\delta\langle Q_{\perp}\rangle=0. \tag{2}$$

By investigating the above condition, termed the *OSM Ansatz*, in more detail [1], it was concluded that OSM is a good approximation when parallel fluxes dominate, parallel conductivity increases strongly with temperature, and the degree of over-/under-ionization on each flux tube does not exceed a factor of two. This means that OSM should be applicable to all SOL regimes, with possible exception of recombination-dominated detachment.

In general, radial information enters OSM along with selected diagnostic data $\varsigma^{\mathrm{diag}}(r)$, whatever this data may be. Cross-field sources $Q_{\perp}$ are then adjusted in order to minimise the error between measured $\varsigma^{\mathrm{diag}}(r)$ and predicted $\varsigma(r)$ quantities

$$\Xi(r)=\frac{\varsigma(r)-\varsigma^{\mathrm{diag}}(r)}{\varsigma^{\mathrm{diag}}(r)}, \qquad \|\Xi\|=\sum_r|\Xi(r)|^2$$
$$\frac{\partial}{\partial\xi(r)}\|\Xi\|\approx 0, \qquad \frac{\partial}{\partial\xi(r)\partial\xi(r)}\|\Xi\|>0 \tag{3}$$

This technique will be referred to as diagnostic variance minimisation (DVM). It is worth noting that DVM is not particular to the OSM, and could be included within existing 2-D fluid codes to increase their diagnostic content and interpretive ability (in that case the specified cross-field transport coefficients would be adjusted in order to minimise the diagnostic variance). Considering only target Langmuir probe data $\{\Gamma_0,\Gamma_L,T_{e,0},T_{e,L}\}^{\mathrm{diag}}$, the two comparison vectors $\varsigma^{\mathrm{diag}}(r)$ and $\varsigma(r)$ become

$$\varsigma^{\mathrm{diag}}(r)=\begin{pmatrix}\Gamma_0^{\mathrm{diag}}(r)\\ \Gamma_L^{\mathrm{diag}}(r)\\ T_{e,0}^{\mathrm{diag}}(r)\\ T_{e,L}^{\mathrm{diag}}(r)\end{pmatrix},$$
$$\varsigma(r)=\begin{pmatrix}\Gamma(r,0)\\ \Gamma(r,L_{\parallel})\\ T_e(r,0)\\ T_e(r,L_{\parallel})\end{pmatrix}=\begin{pmatrix}\frac{1}{m}U^{(2)}(r,0)\\ \frac{1}{m}U^{(2)}(r,L_{\parallel})\\ \frac{2m}{3}U^{(4)}(r,0)/U^{(1)}(r,0)\\ \frac{2m}{3}U^{(4)}(r,L_{\parallel})/U^{(1)}(r,L_{\parallel})\end{pmatrix}. \tag{4}$$

The default cross-field sources for the above case were selected as follows:

$$Q_{\perp}(r,s_{\parallel})=\begin{pmatrix}\xi^{(1)}(r)U^{(1)}(r,s_{\parallel})\\ \xi^{(2)}(r)U^{(2)}(r,s_{\parallel})\\ \Theta(r,s_{\parallel})\\ \Theta(r,s_{\parallel})\end{pmatrix},$$
$$\Theta(r,s)=\begin{Bmatrix}0 & s_{\parallel}\in[0,s_{\parallel}^{X,0}]\\ \xi^{(3)}(r)\gamma_e T_{e,0}^{\mathrm{diag}}\Gamma_0^{\mathrm{diag}} & s_{\parallel}\in[s_{\parallel}^{X,0},\tfrac{1}{2}L_{\parallel}]\\ \xi^{(4)}(r)\gamma_e T_{e,L}^{\mathrm{diag}}\Gamma_L^{\mathrm{diag}} & s_{\parallel}\in[\tfrac{1}{2}L_{\parallel},s_{\parallel}^{X,L}]\\ 0 & s_{\parallel}\in[s_{\parallel}^{X,L},L_{\parallel}]\end{Bmatrix}, \tag{5}$$

where $s_{\parallel}^{X,0}$ and $s_{\parallel}^{X,L}$ are the $s_{\parallel}$ locations of the X-point and $\xi(r)$ are free parameters adjusted in order to minimise the statistical variance between $U(r,s_{\parallel})$ and $U^{\mathrm{diag}}(r)$.

The newly developed onion-skin solver [1] (OSM2) (results from OSM1 were presented at the 13th PSI conference [2]) includes new physics such as: ion viscosity effects, ion–electron collisional energy exchange, smooth supersonic transition, continuous target-to-target solutions, and more accurate treatment of plasma–neutral interactions. The final set of model equations is given below

$$\frac{\partial U}{\partial t}+\nabla_{\parallel}(F_{\parallel}+G_{\parallel})-Q_{\perp}=Q[U],$$
$$Q[U]\equiv Q_{\wp}+Q_{\Im}+Q_B, \tag{6}$$

$$U=\begin{pmatrix}\rho\\ \rho u\\ \rho\varepsilon_i\\ \rho\varepsilon_e\end{pmatrix}, \quad F_{\parallel}=\begin{pmatrix}\rho u\\ p_i+p_e+\rho u^2\\ u(\rho\varepsilon_i+p_i)\\ u(\rho\varepsilon_e+p_e)\end{pmatrix},$$
$$G_{\parallel}=\begin{pmatrix}0\\ \pi_i\\ q_i+u\pi_i\\ q_e\end{pmatrix}, \quad \rho\varepsilon_i=\frac{3}{2}p_i+\frac{1}{2}\rho u^2,$$
$$\rho\varepsilon_e=\frac{3}{2}p_e, \ \ \pi_i=-\eta_i\nabla_{\parallel}u, \ \ q_a=-\kappa_a\nabla_{\parallel}T_a,$$

$$Q_\wp = \begin{pmatrix} 0 \\ 0 \\ -u\nabla_\parallel p_e + \frac{p_e - p_i}{\tau_{ei}^{(2)}} \\ u\nabla_\parallel p_e - \frac{p_e - p_i}{\tau_{ei}^{(2)}} \end{pmatrix},$$

$$Q_B = \left\{ F_\parallel + G_\parallel - \begin{pmatrix} 0 \\ p_i + p_e + \frac{1}{2}\pi_i \\ 0 \\ 0 \end{pmatrix} \right\} \frac{\nabla_\parallel B}{B},$$

$$\eta_i = 0.96 p_i \tau_i, \quad \kappa_i = 3.9 p_i \tau_i / m_i, \quad \kappa_e = 3.2 p_e \tau_e / m_e,$$

where $Q_\perp$ are the cross-field sources, $Q_\wp$ the plasma sources, $Q_\Im$ the neutral sources, Q_B are the magnetic flux expansion terms and $\tau_\alpha \propto m_\alpha^{1/2} T_\alpha^{3/2} n_\alpha^{-1}$. Plasma–neutral interactions enter the model via a neutrals source $Q_\Im$

$$Q_\Im = \begin{pmatrix} m_i(S_{\rm iz} - S_{\rm rec}) \\ m_i(u_{\parallel,H} S_{\rm iz} - u S_{\rm rec}) - m_i(u - u_{\parallel,H}) S_{\rm CX} \\ m_i(\frac{1}{2} u_H^2 S_{\rm iz} - \frac{1}{2} u^2 S_{\rm rec}) + Q_{\rm qi} + Q_{\rm Zi} \\ m_e(\frac{1}{2} u_H^2 S_{\rm iz} - \frac{1}{2} u^2 S_{\rm rec}) + Q_{\rm qe} + Q_{\rm Ze} \end{pmatrix}, \qquad (7)$$

where $S_{\rm iz}$, $S_{\rm rec}$ and $S_{\rm CX}$ are, respectively, the ionization, recombination and charge exchange rates, $u_{\parallel,H}$ is the along-B neutral velocity, u_H the neutral birth velocity, $Q_{\rm qi}$ and $Q_{\rm qe}$ the energy sources for ions and electrons due to plasma–hydrogenic neutral interactions, and $Q_{\rm Zi}$ and $Q_{\rm Ze}$ are similar sources due to plasma–impurity interactions (impurity cooling is estimated by $Q_{\rm Ze} = f_{\rm Ze} Q_{\rm qe}$ and $Q_{\rm Zi} = f_{\rm Zi} Q_{\rm qi}$ with default values of $f_{\rm Ze} = 1$ and $f_{\rm Zi} = 0$; in the future these terms could be calculated iteratively with the impurity transport code DIVIMP [3] within which OSM2 is fully integrated).

Plasma transport equations are discretised on an adaptive parallel grid and in turn solved on each flux surface using a fully- implicit block tri-diagonal inversion with semi-implicit boundary conditions, typical techniques of computational fluid dynamics (CFD). The plasma solution is then transferred onto a coarser poloidal grid and neutral hydrogen transport is simulated using a Monte-Carlo code such as NIMBUS [4] or EIRENE [5]. Neutral sources are then relaxed to assure numerical stability and the cross-field sources are adjusted based on the deviation from desired target conditions. The above OSM2/NIMBUS cycle is iterated until global convergence ensues

$$\begin{array}{lll} \textbf{\textit{Finish}}: & \boldsymbol{U}(\boldsymbol{X}) \overset{\Delta U/U \ll 1}{\leftarrow} \boldsymbol{U}[\boldsymbol{Q}_\Im, \boldsymbol{Q}_\perp] \overset{NIMBUS}{\rightarrow} \boldsymbol{Q}_\Im^{new}[\boldsymbol{U}] & \\ & \textit{CFD} \uparrow & \downarrow \text{relaxation with } \boldsymbol{Q}_\Im^{old}[\boldsymbol{U}] \\ \textbf{\textit{Start}}: \boldsymbol{U}^0, \boldsymbol{Q}_\Im^0, \boldsymbol{Q}_\perp^0 & \rightarrow \boldsymbol{Q}_\perp[\boldsymbol{U}, \boldsymbol{U}^{\rm diag}] \leftarrow & \boldsymbol{Q}_\Im[\boldsymbol{U}] \\ & \textit{DVM} & \end{array}$$

Numerical strategies employed in solving the transport equations and the DVM optimisation problem are described in detail elsewhere [1].

3. Results

The validation of the OSM2/NIMBUS code was carried out in four stages [1]: (a) simulation of all SOL collisionality regimes via a progressive transition from attached to detached conditions (all regimes were successfully simulated, including sheath limited, conduction limited and detached regimes), (b) sensitivity study of the above solutions to cross-field sources (analytical predictions based on the *OSM Ansatz* were confirmed), neutral, plasma, and flux expansion sources, and kinetic boundary conditions sources (agreement with the trends predicted by the modified two-point models was observed), (c) code–code comparison with EDGE2D [6]/NIMBUS [4], (d) code–experiment comparison with reciprocation probe data for Ohmic, L-mode and H-mode discharges for JET MkIIGB. The full set of results (a)–(d) is reported elsewhere [1]; below, we summarise the results of code–code (c) and code–experiment (d) comparisons and present an OSM2/NIMBUS simulation of a JET MkIIGB 12 MW ELMy H-mode discharge with total power profiles extracted via a gradual X-point shift [7].

3.1. Code–code comparison (OSM2/NIMBUS vs EDGE2D/NIMBUS)

Target conditions $(J_{\rm sat}, T_e)$ from a low power EDGE2D/NIMBUS solution ($P_\perp^{\rm sep} = 1$ MW, $n_{\rm sep} = 0.5 \times 10^{19}$ m^{-3}, $D_\perp = 0.15$ m^2 s^{-1}, $\chi_\perp^i = 1$ m^2 s^{-1}, $\chi_\perp^e = 1$ m^2 s^{-1}, $\gamma_e = 5.0$, $\gamma_i = 2.5 + M_0^2(T_{e,0} + T_{i,0})/(2T_{i,0})$) were used to obtain an OSM2/NIMBUS solution, Fig. 1. Special care was taken to insure that OSM2 and

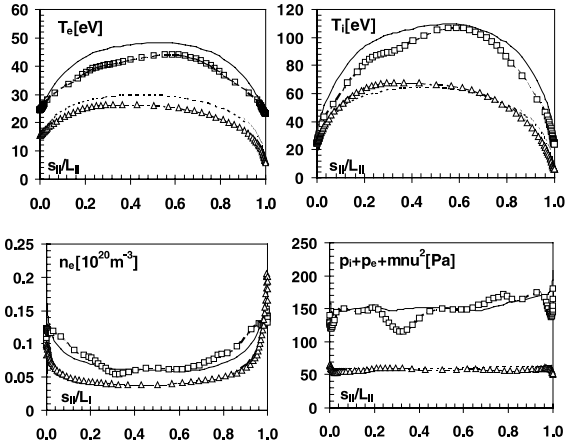

Fig. 1. Comparison of OSM2 (solid and dotted lines) and EDGE2D (squares and triangles) for two radial locations, $r_{\rm mid} = 1$ mm and 15 mm. $S_\parallel$ is the distance along the field line measured from the outer target; $L_\parallel$ is the target-to-target connection length.

EDGE2D modeling equations differed only in the treatment of radial fluxes: (a) neutral sources, including Q_{CX} and Q_{qi}, were calculated directly by NIMBUS, (b) impurity contributions were neglected, $f_Z = 0$, (c) the same kinetic boundary conditions $\{\gamma_e, \gamma_i\}$ were used, (d) flux limited heat conductivities were replaced by classical values. Comparison reveals close agreement between the OSM2 and EDGE2D solutions, despite strong parallel and perpendicular gradients (the near target drop of separatrix p_{tot} in the EDGE2D solution is accompanied by spatial oscillation which has been linked to coarseness of the poloidal grid near the target). The diffusivities $\chi_{\perp(i,e)}$ used as input by EDGE2D were recovered by OSM2 to within 20%.

3.2. Code–experiment comparison (OSM2/NIMBUS vs RCP measurement)

RCP measurements of T_e and n_e radial profiles in the upstream SOL were compared with the predictions of OSM2/NIMBUS (based on target probe profiles) for over 20 JET MkIIGB discharges [8] (Ohmic, L-mode, H-mode), producing agreement to within the experimental error of ~20%, except for the poor agreement in Mach number (drift effects are not included in OSM2, although momentum sources are introduced to compensate for pressure asymmetries). A comparison for a typical L-mode discharge is shown in Fig. 2. Because of uncertainty in the position of the separatrix, the profiles were shifted to obtain total pressure balance (typical shift ~20 mm). The OSM2 extracted flux-surface averaged cross-field heat diffusivities for ions and electrons, $\chi_{\perp(i,e)}$ are also shown in Fig. 2. The general trend is for $\chi_{\perp(i,e)}$ to increase away from the separatrix and for the value at the separatrix $\chi_{\perp,sep}$ to decrease with power entering the SOL [8], i.e., $\chi_{\perp,sep} \propto P_{sol}^{-1.1}$ and $\lambda_p \propto P_{sol}^{-0.5}$. This observation stands in contradiction to most theories, which predict an increase of $\chi_\perp$ with P_{sol}; a possible explanation for this scaling will be put forward in the following section.

3.3. OSM2/NIMBUS simulation of a JET MkIIGB 12 MW ELMy H-mode (X-point shift experiment)

In order to measure the SOL power width in ELMy H-mode, a repeated 12 MW discharge (2.5 MA, 2.5 T, $\langle n_e \rangle \sim 6 \times 10^{19}$ m^{-3}) was formed with different X-point height. Based on embedded thermocouples (TC), the total power $q_\parallel^{tot}$ radial profile was extracted for both the inner and outer targets, in addition to the electron power $q_\parallel^e$ profile from target probes; the details of the experiment and the thermal analysis are described in a paper presented at this conference by Matthews [7]. The resulting profiles show a very thin power width at the outer target only, $\lambda_p \sim 2$ mm, with a corresponding peak parallel heat flux of ~250 MW m^{-2} (cf. inside ~40 MW m^{-2}). For the OSM2 analysis, $q_\parallel^e(r)$ was constrained (via Γ and T_e), while the ion to electron input power ratio P_i/P_e was adjusted to match $q_\parallel^{tot}(r)$; $P_i/P_e \sim 10$ was needed to match outer $q_\parallel^{tot}(0)$. With this ratio, the inner $q_\parallel^{tot}(r=0)$ is greatly overestimated. For $P_i/P_e = 10$, OSM2 predicts $n_{eu} \sim 1 \times 10^{19}$ m^{-3}, $T_{eu} \sim 80$ eV, $T_{iu} \sim 350$ eV, so that $\nu_i^* \ll \nu_e^*$ (since $\nu^* \propto n/T^2$); near the separatrix $\nu_e^* \sim 20$ (collisional electrons), while $\nu_i^* < 1$ (collisionless ions), implying direct ion orbit losses. Based on results of a guiding centre orbit following code ORBIT-M [9], ion orbits terminate preferentially at the outer target with $B \times \nabla B$ towards the X-point and at the inner target with reversed $B \times \nabla B$. Therefore, we expect the narrow peak in $q_\parallel^{tot}(r)$ to shift to the inner side with reversed $B \times \nabla B$ (due to longer connection length from the outer midplane to the inner target, substantial attenuation and broadening may occur). Extracted $\chi_{\perp i}$, $\chi_{\perp e}$, Fig. 3, agree with the Bohm estimate (1–3 m^2 s^{-1}) in the outer SOL, but drop rapidly towards the separatrix (<0.3 m^2 s^{-1}). The absolute value is in good agreement with neo-classical plateau estimate of $\chi_{\perp i}$ (note that plateau transport is the lowest neo-classical regime which could be active in the edge, since banana orbits are by definition closed and provide no direct losses). This suggests that the

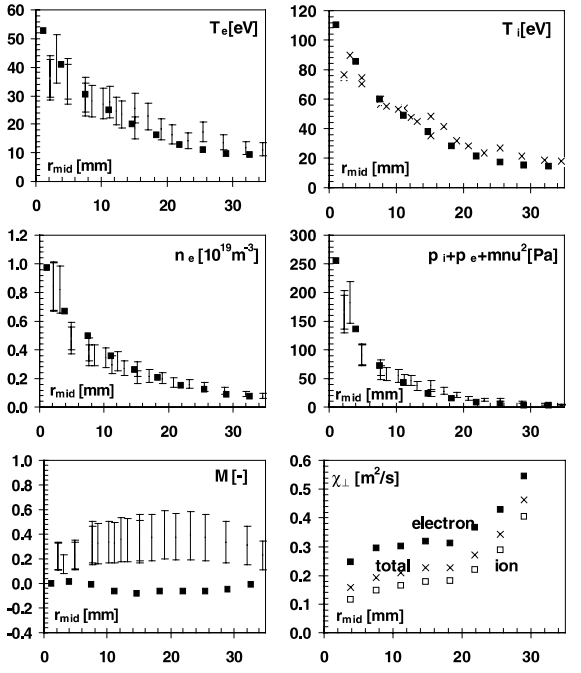

Fig. 2. Comparison of OSM2/NIMBUS solutions (squares) with RCP measurements (vertical error bars) for JET shot 45791 at $t = 63$ s (L-mode, $P_{in} = 3$ MW); r_{mid} is the radial distance from separatrix at the outer mid-plane. Since ion temperature is not measured, it was assumed that $T_i^{RCP} = T_e^{RCP}(T_i^{OSM}/T_e^{OSM})$.

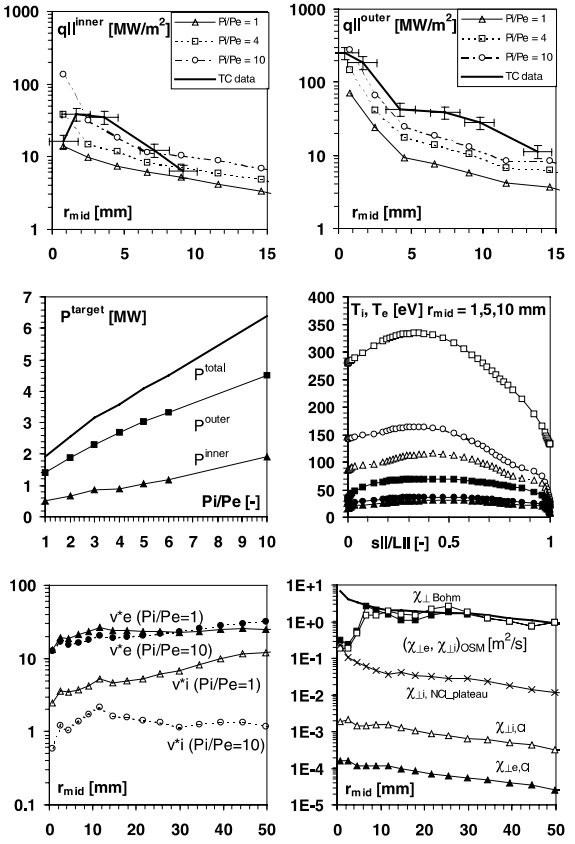

Fig. 3. Inner–outer target heat fluxes (ions and electrons) as calculated by OSM2/NIMBUS for different values of Pi/Pe, compared to heat fluxes extracted from TC during the *X*-point shift experiment; total power to inner and outer targets; plasma temperatures vs field line distance from outer target at three radial locations in the SOL; normalised collisionalities; cross-field heat diffusivities extracted from OSM2 compared to theoretical values.

H-mode transport barrier (ETB) extends beyond the pedestal region into the SOL. Assuming that ion orbit losses are responsible, the width of high power region can be estimated as $(\chi^i_{\perp\mathrm{neo}}\tau_{\min})^{1/2}$, where $\tau_{\min} = \min(\tau_\parallel, \tau_{\mathrm{coll}})$ with parallel loss time $\tau_\parallel = (L_\parallel/2v_t)$ and decorrelation time $\tau_{\mathrm{coll}} = v_{ii}/(r/R)^{3/2}$, which gives ~2–3 mm (cf. $\lambda_{\mathrm{p}}^{\mathrm{outer}} \sim 2$ mm). In the emerging picture, $q_\perp^{\mathrm{tot}}(r)$ would be determined chiefly by the degree of ion collisionality v_i^*: (a) when $v_i^* \gg 1$, transport is driven by local turbulence, (b) as v_i^* decreases towards unity, ion orbits penetrate closer to the outer target before suffering a collision, which tends to reduce $\lambda_{\mathrm{p}}^{\mathrm{outer}}$ and $\chi_{\perp i} \equiv q_{\perp i}/\nabla T_i$. In other words, we suggest that the observed scaling at JET [8] ($\chi_\perp \propto P_{\mathrm{sol}}^{-1.1}, \lambda_{\mathrm{p}} \propto P_{\mathrm{sol}}^{-0.5}$) reflects the change in ion collisionality and the associated rise in orbit losses rather than any intrinsic scaling of turbulent or neo-classical transport (both of which increase with T_i and hence with P_{sol}). This idea will be pursued further in a separated publication.

4. Conclusions

The advanced onion-skin solver (OSM2/NIMBUS) has passed several levels of code validation: (a) it agrees with the theoretical predictions based on variational analysis, (b) it follows the basic trends predicted by the two-point model in attached conditions, (c) it captures all SOL regimes (sheath limited, high recycling, detached), (d) it shows good agreement with a standard 2-D fluid code (EDGE2D/NIMBUS), (e) it reproduces to within 20% RCP profiles on Ohmic, L-mode and H-mode shots on JET MkIIGB. In addition, it offers spatial information about radial transport in the SOL; for the *X*-point shift experiment (12 MW ELMy H-mode) where both electron and total power profiles at the targets were measured, it leads to new insights about the underlying mechanism (ion orbit loss) of the observed narrow power width and in–out asymmetries. OSM analysis is expected to be used extensively in the upcoming JET campaigns; future developments will focus on extending the diagnostic set used to constrain the OSM2 solution, model strongly detached discharges by constraining D_α emission and first attempts at modelling time-dependent phenomena such as fluctuations and ELMs.

References

[1] W. Fundamenski, Ph.D. Thesis, U. Toronto, 1999.
[2] W. Fundamenski et al., J. Nucl. Mater. 266–269 (1999) 1045.
[3] P.C. Stangeby, J.D. Elder, Nucl. Fus. 35 (1995) 1391.
[4] E. Cupini, A. De Matteis, R. Simonini, NET Rept. EUR XII (1984) 3249.
[5] D. Reiter, Julich Report 1947 (1984).
[6] R. Simonini et al., Contrib. Plasma Phys. 34 (1994) 368.
[7] G.F. Matthews, these Proceedings.
[8] S.K. Erents et al., Nucl. Fus. 40 (2000) 309.
[9] A.V. Chankin, G.M. McCracken, Nucl. Fus. 33 (1993) 1459.